"The Feasibility of a Cochlear Nucleus Auditory Prosthesis Based on Microstimulation"

Contract No. NO1-DC-5-2105

QUARTERLY PROGRESS REPORT #2

October 1, 1995 to December 31, 1995

HOUSE EAR INSTITUTE

2100 W. Third St.
Los Angeles, CA 90057

R.V. Shannon, Ph.D.
J. Moore, Ph.D.
J. Huang, B.S.
M. Chatterjee, Ph.D.
F. Portillo, B.S.E.
B. Wu, B.S.

HUNTINGTON MEDICAL RESEARCH INSTITUTES

Neurological Research Laboratory
734 Fairmount Ave
Pasadena, CA 91105

D.B. McCreery, Ph.D.
W.F. Agnew, Ph.D.
T.G.H. Yuen, Ph.D.
L.A. Bullara, B.S.

Draft March 4, 1996

TABLE OF CONTENTS

1.0 SUMMARY AND ABSTRACT

The overall goal of this contract is to develop an auditory prosthesis based on multisite microstimulation within the cochlear nucleus (CN). Section 2 deals with issues related to specifications of a microelectrode array designed to fit the human cochlear nuclear complex. Section 3 describes the development of computer models for designing a tool for intrasurgical implantation of the microelectrode array. Because the current work in both of these areas is based on investigations carried out during the first and second contracts (1989-92 and 1992-95), we include a brief summary of our previous work in these areas. Section 3 will describe experiments designed to characterize the neural activation produced by electrical stimulation of microelectrodes in the CN of an animal model. Section 4 will describe studies to evaluate the penetration forces necessary to insert electrodes through the pial-glial covering over the human CN.

2.0 DESIGN OF A COCHLEAR NUCLEUS ELECTRODE ARRAY

A continuing issue in the development of brainstem auditory microelectrodes has been the fit of the electrode to its target, the cochlear nuclei. The work statement charges us with drawing up specifications for the optimal number, size, spacing and orientation of electrodes within the array. This can only be done on the basis of modeling the size, shape and volume of the human cochlear nuclear complex. More specifically, it needs to be based on material from subjects who have developed large acoustic neuromas which disrupt the cochlear nerve and distort the normal morphology of the cochlear nuclei.

2.1 Previous Work in Nuclear Shape

In QPR #4 of the first contract, we compared the overall size and shape of the cochlear nuclei in a hearing subject and in our first profoundly deaf subject. At that time we saw no difference between the two subjects in terms of nuclear shape and size, but we noted that in both brains, the maximum diameter of the ventral cochlear nucleus (VCN) was 2-4 mm in any dimension. By QPR #8, we had digitized the outlines of the cochlear nuclei in seven normal subjects of different ages and eight profoundly deaf subjects. The population of deaf subjects included one with a unilateral neuroma, but no neurofibromatosis (NF2) subjects. Again, no differences were noted in nuclear shape and gross size in the hearing and deaf subjects. At that time we pointed out that the only surface landmarks for the position of the VCN are the roots of the 7th (facial) and 8th (vestibulocochlear) cranial nerves.

In QPR #12 of the first contract, we used the brainstem of our first NF2 subject to produce a three-dimensional reconstruction of the cochlear nuclei and surrounding structures, including the vestibular nuclei, somasthetic pathways, facial nucleus and nerve, cerebellar flocculus and peduncles, and brainstem surface. This subject had died of a condition unrelated to his NF2 prior to the time that the tumors became large enough to necessitate surgical removal. This brainstem did not, therefore, show any distortion of the cochlear nuclei or of neighboring structures. We used this reconstruction of the brainstem as the basis for a scale model of a single shaft electrode, and determined that the shaft should be about 5 mm long, with electrode sites on the distal 3 mm which fell within the VCN. The proximal 2 mm of the shaft passed through noncochlear tissue and were not modeled with electrode sites. We also used this reconstruction to predict the results of insertion of the electrode shaft into an incorrect location or at an incorrect angle. In both cases, the structures pierced by the shaft were cerebellar, either the flocculus or the middle peduncle.

By QPR #4 of the second contract, we had received the brainstem of a second NF2 subject who had undergone bilateral removal of acoustic neuromas and implantation of a brainstem surface electrode (ABI). In this subject, unlike all previous deaf subjects, there was some distortion and flattening of the cochlear nuclei on both sides. We hypothesized that this change in shape could have been caused either by pressure from the tumors on the brainstem or by the loss of all eighth nerve terminals in the cochlear nuclei, causing a severe reduction in tissue volume. This brainstem was also used for a three dimensional reconstruction of the pontomedullary region of the brainstem, including the cochlear nuclei and surrounding structures.

2.2 Previous Work in Nuclear Volume

The series of studies carried out to investigate volume of the cochlear nuclei confirmed our assumptions about change in the operated NF2 case. In QPR #8 of the first contract, we reported nuclear volume for five normal and five profoundly deaf subjects. The data was obtained by digitizing drawings of individual histological sections into the PC3D (Jandel) program, which creates three dimensional reconstructions and calculates volumes. The nuclear volume in the normal subjects varied with age, rising to age 50-60 and then subsequently declining, as predicted by previous work of other investigators. The volume of the cochlear nuclei of the profoundly deaf non-NF2 subjects were not different from the volume of age matched subjects with normal hearing. In QPR #6 of the second contract, we examined the cochlear nuclei of the operated NF2 subject and found them to be only one-half to two-thirds the size of those of an age-matched normal subject. This presents a significantly smaller target for electrode insertions. Therefore we proposed that electrode design should be done on the basis of reconstruction of the cochlear nuclei from neuroma surgery patients, preferably those with NF2.

2.3 Current Work: Modeling the Cochlear Nuclei and Brainstem Surface

All of our work on reconstruction of the cochlear nuclei, other than the earliest drawings, has been done on the isolated nuclear complex. Final design of an electrode array will require three-dimensional reconstruction of both the nuclei and the overlying tissue through which the electrode shaft(s) must pass. Figures 2.3a-c illustrate sections which have been digitized into PC3D and transferred into AutoCAD for this purpose. Figures 2.3a and 2.3b are derived from the brainstems of subjects with surgically removed unilateral neuromas (89-54 and 92-10). Figure 2.3c shows the brainstem of the bilaterally operated NF2 subject (92-13). In all cases the left cochlear nuclear complex was digitized. The right side of the NF2 subject (92-13) received an ABI device, which distorted the brainstem surface and made the tissue unusable for this project.

Several conclusions can be drawn on the basis of the individual sections. First, there is an extremely high degree of variability in size and shape across subjects, higher than previously seen in normal and non-NF2 deaf subjects (e.g., first contract, QPR #8). This means there will be very little predictability of the size and shape of the VCN segment an electrode is targeting. Secondly, in using the 8th and 7th nerve roots as a guide to the nucleus, the electrode must be inserted lateral to the nerve roots (indicated by open arrows in all figures). In all cases, this limits the segment of the nucleus available for implantation to the anterior half of the nucleus (AVCN). This may have implications for electrode effectiveness, since two investigators working with microelectrodes in the mammalian cochlear nuclei have found that transmission to the inferior colliculus is more efficient from the posterior VCN than from its anterior half (H. El Kashlan and D. McCreery, personal communications).

A practical consideration is the volume of tissue available for stimulation if the electrode is inserted in relation to the 7th and 8th nerve roots. These segments are indicated in black in all figures, while the remainder of the complex, primarily the dorsal and posteroventral nuclei, is crosshatched. In subject 89-54, the section spacing is 375 μm, which creates a AVCN segment with a total length of about 1000 μm (1.0 mm) available for implantation. In subjects 92-10 and 92-13, the section spacing is 300 μm. In subject 92-10, the available segment of the nucleus is only about 600 μm, or slightly more than half a millimeter, because the flocculus covers the surface anteriorly (section 346) and precludes electrode

insertion. In the NF2 subject, 92-13, the length of the available AVCN segment is approximately 900 μm. These limited dimensions, combined with the irregularity of AVCN shape, probably make it unlikely that a single-shaft electrode could reliably hit the nucleus. Thus it may be necessary to consider a "pitchfork" or grid design which incorporates several shafts, each carrying multiple electrode sites.

In the next work period, these three AVCN segments will be modeled in three dimension to ascertain the exact shape and volume of tissue into which a single- or multishaft electrode array could be placed. These models will include the alignment of isofrequency planes in the AVCN. This will allow us to set the limits of the dimensions of the electrode array.

3.0 DESIGN OF AN INSERTION TOOL

A second goal is consideration of the surgical route for reaching the target, the cochlear nuclei. Section D2 of the work statement charges us to design a tool or set of tools permitting safe and convenient insertion of the electrodes into the VCN in relation the tonotopic gradient. This requires modeling of the cochlear nuclei and surrounding brainstem structures in combination with the skull and head surface.

3.1 Previous Work in Radiological imaging

In QPR #4 of the first contract, we described studies of radiologic imaging of a cadaver head. In this study, an HEI research physician, Dr. Jose Fayad, created translabyrinthine openings bilaterally on the head. The head was then imaged by both computerized tomography (CT) and magnetic resonance imaging (MRI). Prior to imaging, the VCN was labeled with marker substances (metal wire for CT and gadolinium injection for MRI). Because of the small volume of tissue investigated, special techniques were used in both types of imaging. For CT, slice thickness of 1.5 mm was obtained and sections were overlapped to produce images at 1 mm intervals. For MRI, images were produces by a T1 weighted spin echo technique. The resulting images were remarkably clear and allowed us to match anatomical and radiological landmarks. This included identification of the pontomedullary region of the brainstem, the ventral cochlear nucleus, the fourth ventricle and lateral recess, the cerebellar flocculus, and the 5th, 7th and 8th nerves.

3.2 Previous Work in Whole Head Modeling

During the second contract, we developed hardware and software for three dimensional reconstruction and manipulation of images of the entire head. As previously mentioned (section 2.1) and described in QPR #4 of the second contract, we reconstructed the brainstem segment of the operated NF2 subject in the PC3D program. A program, 3D2CAD.EXE, was developed for transferring the PC3D images into the AutoCAD system. In QPR #6, we reported fitting the reconstructed brainstem into a generic head/skull/brain model from Viewpoint Datalab. Both the head surface and skull modules of this generic head consisted of removable polygons. As reported in QPR #8, we collaborated with the neurosurgeon, Dr. William Hitselberger, to delete meshes of the head surface and skull and thus create a "surgical opening". We were able to visualize this conical opening in lateral, axial and anteroposterior planes of section in wire frame and solid images. At this time, we made the first model of in an insertion tool, indicating the length and angle in the distal portion of the tool, which would be necessary to reach the VCN. Because our model included the orientation of

isofrequency planes in the VCN, we could determine if the electrode would traverse the tonotopic gradient of the nucleus.

In QPR #12 (final report) of the second contract, we reported that we had reached the limits of accuracy of the generic head model, since it did not provide the internal surface of the skull or any meningeal or vascular structures. In order to achieve greater accuracy, we decided to return to radiologic images. At that time, we reported that we had acquired 24 CT scan sections of a cadaver head with translabyrinthine surgical openings. The original 9 track magnetic tape from the CT scan was brought into a Unix SPARC station equipped with a tape drive. A C program was used to reformat the files and extract the images, which were than transferred into the NIH Image program. This program has the capacity to trace the edges of the structures and save the edge, or wire frame, files in DXF format. These files can then be utilized in AutoCAD for three dimensional reconstruction.

3.3 Current work: Modeling the Surgical Opening

Figures 3.3a-c are examples of the reconstructions produced by this method, progressing from a single "edge" section (Fig. 3.3a) through series of stacked wire frame images (Figs. 3.3 a-b) to shaded models (Fig. 3.3c). The upper image in Figure 3.3 is a single edge image which illustrates the component modules of the figure. It includes the head surface (in grey) with the ear reflected forward because of the postauricular surgical approach. The skull (in white) includes the frontal, temporal and occipital bones: it also shows the wing-shaped extension of the temporal bone forming the petrous pyramid which contains the inner ear. The defect in the skull represents the translabyrinthine surgical opening. The posterior fossa of the skull contains the brainstem and cerebellum (in grey). Running from the brainstem surface are the trigeminal (5th) nerve in blue and the facial-vestibulocochlear (7th-8th) nerves in red. The dural layers and enclosed venous sinus are represented in yellow.

Nine stacked edge, or wire frame, images are shown in the lower image of Fig. 3.3a. The reconstruction includes the modules for head surface, skull, brainstem-cerebellum and the dura enclosing the jugular bulb (in yellow). It represents a level below that of the ear, vestibulocochlear nerve and cochlear nuclei, and demonstrates the structures that form the floor of the translabyrinthine opening. Figure 3.3b shows two higher levels of reconstruction. In the upper image, five sections have been added. The 7th-8th nerve bundle (in red) is seen emerging from the posterior surface of the petrous pyramid. In the lower image, five more sections have been added. This reconstruction shows the entire 7th-8the nerve bundle (in red) and the more rostrally located trigeminal nerve (in blue). Figure 3.3c shows a shaded reconstruction of the skull, dura, and cranial nerves derived from the wire frame images. The top image is a view through the translabyrinthine opening from the lateral surface of the head, i.e., from the surgeon's viewpoint. The lower image shows the same reconstruction from above, in order to illustrate the depth of the surgical approach and the configuration of the internal structures. The accuracy of the reconstructed figure is indicated by the fact that it conforms to the surgeon's description of the surgical opening: (QPR #4 of first contract) as bounded by the dural tentorium superiorly, the sigmoid sinus posteriorly, the jugular bulb inferiorly and the facial nerve and bone surrounding the auditory structures anteriorly.

The studies described in Section 2 of this report make it clear that placement of an electrode into the ventral cochlear nucleus will require the electrode to penetrate the brainstem surface just lateral to the 7th-8th nerveroots

and orthogonal to the brainstem surface. In the next contract period, we will use this reconstruction, possibly with placement into the generic head, to determine the geometry of an insertion tool that can correctly position the electrode array.

4.0 PENETRATION FORCE STUDIES

The human cochlear nucleus is covered by a tough pial-glial layer that presents a difficult problem for penetrating microelectrodes. It is unknown at the present time how much force is required to insert penetrating microelectrodes through this layer into the underlying cochlear nucleus. We have designed a computer-controlled mechanical insertion device to control the insertion speed and to record the actual forces necessary for penetrating the pial layer with different types of microelectrodes. Our initial tests of this system revealed problems with mechanical artifacts, which we have now corrected. Figure 4-1 shows a record of a sample penetration of a Platinum-Iridium HMRI electrode into fresh human brainstem tissue. The record plots two traces as a function of time: (1) position of the electrode in mm, and (2) force in grams. The position trace shows the acceleration and distance travelled by the motorized electrode carrier. The force measured during the penetration is shown in the other trace. An insertion at low speed (0.635 cm/sec) is shown in the upper panel and a rapid insertion speed (6.35 cm/sec) in the lower panel. In the upper panel note that as the electrode tip encounters the tissue there is an increase in force. There is a buildup in force over a short time period that probably represents deformation (or dimpling) of the tissue surface, prior to the electrode tip penetrating through the tough pial layer. Once the electrode penetrates the pial layer the force is reduced. At 6.35 cm/sec the force measurements show a large oscillation when the machine starts and stops. This oscillation obscures the profile of force during initial contact with the tissue and subsequent penetration. Subsequent tests should show the oscillation to arise from the vibration of the entire machine due to the abruptness of the acceleration in the stepper motor.

The stepper motor acceleration profile has been reprogrammed to a sinusoidal function, thus avoiding the abrupt transitions. New force measurements show that the artifactual vibratory force profiles are eliminated by this change.

We have obtained fresh, unfixed human brainstems and have prepared them for insertion force measurements. Insertion forces will be measured for as a function of acceleration profile for HMRI Iridium electrodes in the next quarter. Preliminary tests will also be conducted with University of Michigan probes. We are working with the University of Michigan electrode design team to specify a design that may have the necessary shaft strength and tip sharpness for this application.

5.0 PHYSIOLOGICAL RECORDINGS

Multi-unit neural responses and evoked potential responses were recorded in the cat inferior colliculus (IC) in response to electrical pulses delivered at a series of dorsoventral locations in the contralateral posteroventral cochlear nucleus (PVCN). Responses were recorded for several stimulating microelectrode locations in the PVCN and for several stimulating current levels. Post-stimulus time histograms were recorded every 200 microns as the electrode was advanced dorsolateral to ventromedial along the tonotopic axis of the inferior colliculus. The

resulting data is presented in the form of a neural spectrogram, i.e., tonotopic position (depth) vs. time.

5.1 Physiology: Method

PREPARATION: Cats were anesthetized with Halothane and nitrous oxide. A stimulating microelectrode was advanced into the left posteroventral cochlear nucleus (PVCN) after resection of part of the flocculus of the overlying cerebellum. An iridium recording microelectrode was advanced into the contralateral inferior colliculus (IC) after resection of part of the overlying occipital lobe of the cerebral cortex. The evoked response and multi-unit neuronal activity were recorded at intervals of 100 mm (CNA3) or 200 mm (CNA4 and CNA5) along the tonotopic axis of the IC (dorsoventral in CNA3, dorsolateral to ventromedial in CNA4 and CNA5: 45 degree angle from midline). The sequence of measurements in the IC was repeated with the stimulating electrode at 3 or 4 locations along the dorsoventral extent of the PVCN. Response patterns were collected from eight (CNA3), seven (CNA4), or five (CNA5) separate penetrations in the IC in a lateral-to-medial plane.

STIMULI: Controlled-current, charge-balanced, triphasic pulses (cathodic phase 150 msec duration) and 8 to 24 μA in amplitude were delivered at a 20 Hz rate through the stimulating microelectrode in the PVCN. The signal from the recording electrode was sent through a band-pass filter: 2 to 10 kHz for multi-unit activity, and 250 to 2200 Hz for gross evoked potentials. The recording amplifier was blanked for the first 300 msec to avoid overloading by the electrical stimulus artifact. Responses were averaged over 300 stimulus presentations for CNA3, and 512 repetitions for CNA4 and CNA5. For evoked response recording the amplitude of the first large negativity was used as the index of neuronal activity. The negativity of the evoked response will be maximum when the recording electrode is in the center of the region of maximum evoked neuronal activity. The threshold level for multi-unit recording was readjusted at each recording depth to compensate for changing levels of spontaneous activity.

HISTOLOGY: At the end of the experiment the stimulating and recording microelectrodes were fixed in place relative to the skull by flooding the craniectomies with melted dental wax. The cat was deeply anesthetized with Pentothal and perfused through the heart with fixative (1/2 strength Karnovsky's solution) so that the location of the recording and stimulating electrodes could be identified in histologic sections.

5.2 Physiology: Results

Figure 5-1 presents multi-unit, post-stimulus-time (MU-PST) histograms of IC activity for four stimulus levels (8, 12, 16, and 24 μA) as a function of penetration depth in the IC. The individual panels can be interpreted as analogous to a spectrogram, plotting frequency (tonotopic place) on the vertical axis and time after the stimulus pulse on the horizontal axis (Harris et al., 1990). Color indicates the level of MU activity at a particular post-stimulus time and IC depth. The top of each panel is the MU-PST from the dorsal (low frequency) portion of the IC and successive pixel traces are from successive deeper levels (higher frequency locations) in the IC. The total distance of each penetration is given in the upper right of the panel. Multiple response epoches are observed from a single electrical triphasic pulse, with the initial latency of 2-3 ms and an interpeak interval of 0.3-0.7 ms. The time of the response peaks in animal CNA3 (not shown) changed as a function of depth in the IC. The response peaks in Figure 5-1 (CNA4) are nearly vertical, indicating nearly synchronous firing of the neural units at all depths in the

IC. We infer from the difference between the responses in CNA3 and CNA4 that the delay between peaks changes as a function of dorsomedial to ventrolateral position in the IC, as suggested by Langner and colleagues. This could indicate a systematic difference in the path length of projections from PVCN to IC or a systematic difference in the time constant of oscillatory feedback intrinsic to the pathways.

Figures 5-2 and 5-3 show IC rate profiles at 16 μA for CNA3 and CNA4 as a function of IC depth with stimulating location in the PVCN as a parameter. The top panel is evoked responses and lower panel is from multi-unit responses. Note that the peak response in IC shifts systematically as the location of the stimulating electrode is changed in the PVCN. EP curves are wider than the MU curves, which is expected due to the larger effective recording distance of the EP method.

Figure 5-4 plots the peak response location in the IC for CNA3 (top) and CNA4 (lower) as a function of stimulating electrode location in the PVCN. Note the systematic change in the location of peak response activity as the stimulating electrode is moved.

Figure 5-4 shows a MU intensity series from CNA4, i.e. the spatial distribution of MU activity in the IC as a function of depth for four intensity levels of electrical stimulation.

5.3 Physiology - Discussion

These results demonstrate that penetrating microelectrodes can stimulate localized regions in the PVCN and that tonotopic selectivity is preserved as the neural activity propagates to the level of the IC. MU-PST response patterns show a complex temporal response. A single triphasic electrical pulse produces multiple bursts of highly synchronized responses. Both the latencies of the initial response and the inter-burst latencies suggest a regular organization of projections from PVCN to IC. At least three possibilities exist to account for such repetitive response patterns. (1) The multiple response peaks could indicate multiple pathways differing in length from the stimulated region of the PVCN to the IC. (2) Pathways may differ in the number of intervening synapses. (3) A single pathway may have a recurrent feedback loop which functions as an autocorrelator circuit. Langner (1983, 1992) has proposed such a circuit for extracting temporal regularity, such as modulation or temporal pitch. Furthermore, Langner and Schreiner (1988) demonstrated a difference in the time constant of the autocorrelator as a function of dorsomedial-ventrolateral location in the IC orthogonal to the tonotopic axis. The results from our experiments in three animals are consistent with this concept.

The dynamic range of response to electrical stimulation appears to be greater than 10 dB, since thresholds are about 8 μA and little saturation is observed at 24 μA (FIGURE 6). This suggests that penetrating electrode stimulation can provide control of intensity and dynamic range comparable to cochlear implants and surface electrode brainstem implants.

5.4 Physiology - Conclusions

1. Tonotopically selective electrical stimulation of the PVCN is possible with penetrating microelectrodes.

2. Tonotopic specificity is preserved at the IC level with localized electrical stimulation of the PVCN.

3. Latencies of initial IC responses suggest that both direct and multiple synaptic pathways are activated by electrical stimulation of PVCN.

4. Periodic activation of neural units in the IC in response to single electrical pulses in the PVCN suggests either multiple pathways or intrinsic oscillatory pathways.

5. These results were presented at the Association for Research in Otolaryngology Midwinter Meeting in February 1996 (Shannon et al., 1996).

6.0 REFERENCES

Harris, D.M., Lambert, D., and Shannon, R.V. (1990). Trade-off between spatial and synchrony representations of stimulus frequency in the gerbil IC, Abstracts of the ARO Midwinter Research Meeting, (D.J. Lim, Ed.).

Langner, G. (1983). Evidence for neuronal periodicity detection in the auditory system of the guinea fowl: Implications for pitch analysis in the time domain, Exp. Brain Res., 52, 333-355.

Langner, G. (1992). Periodicity coding in the auditory system, Hearing Research, 60, 115-142.

Langner, G. and Schreiner, C.E. (1988). Periodicity coding in the inferior colliculus of the cat. I. Neuronal mechanisms, J. Neurophysiol., 60, 1799-1822.

Schriener, C.E. and Langner, G. (1988). Periodicity coding in the inferior colliculus of the cat. II. Topographic organization, J. Neurophysiol., 60, 1823-1840.

Shannon, R.V. McCreery, D., Chatterjee, M., and Synder, R. (1996). Spatial and temporal multi-unit response patterns in the inferior colliculus produced by electrical stimulation of the cochlear nucleus, **ARO Midwinter meeting**, St. Petersburg Beach, Florida, Feb 4-8, 1996.

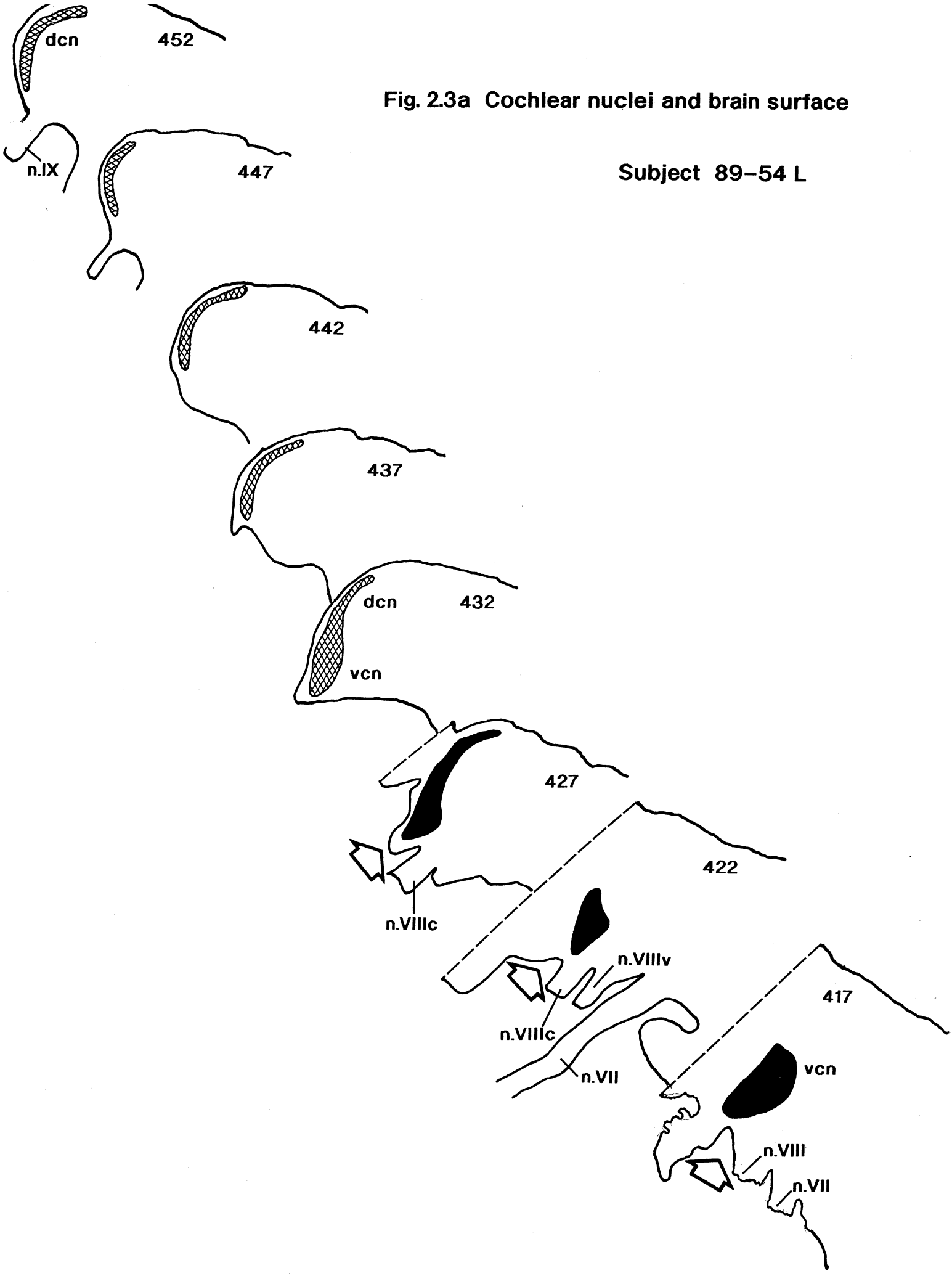

Fig. 2.3a Cochlear nuclei and brain surface

Subject 89–54 L

Fig. 2.3b Cochlear nuclei and brain surface

Subject 92–10 L

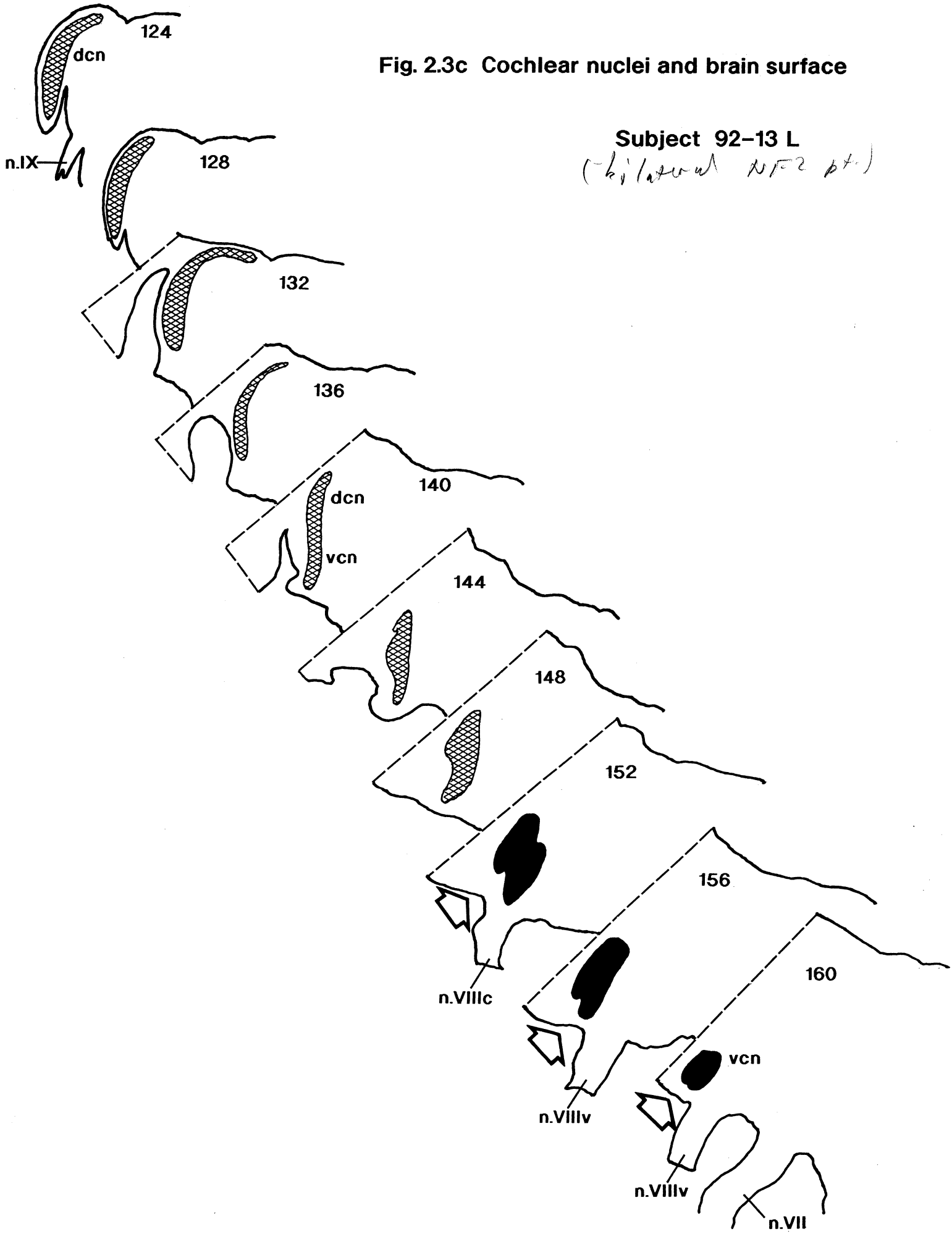

Fig. 2.3c Cochlear nuclei and brain surface

Subject 92-13 L

(bilateral NF2 pt.)

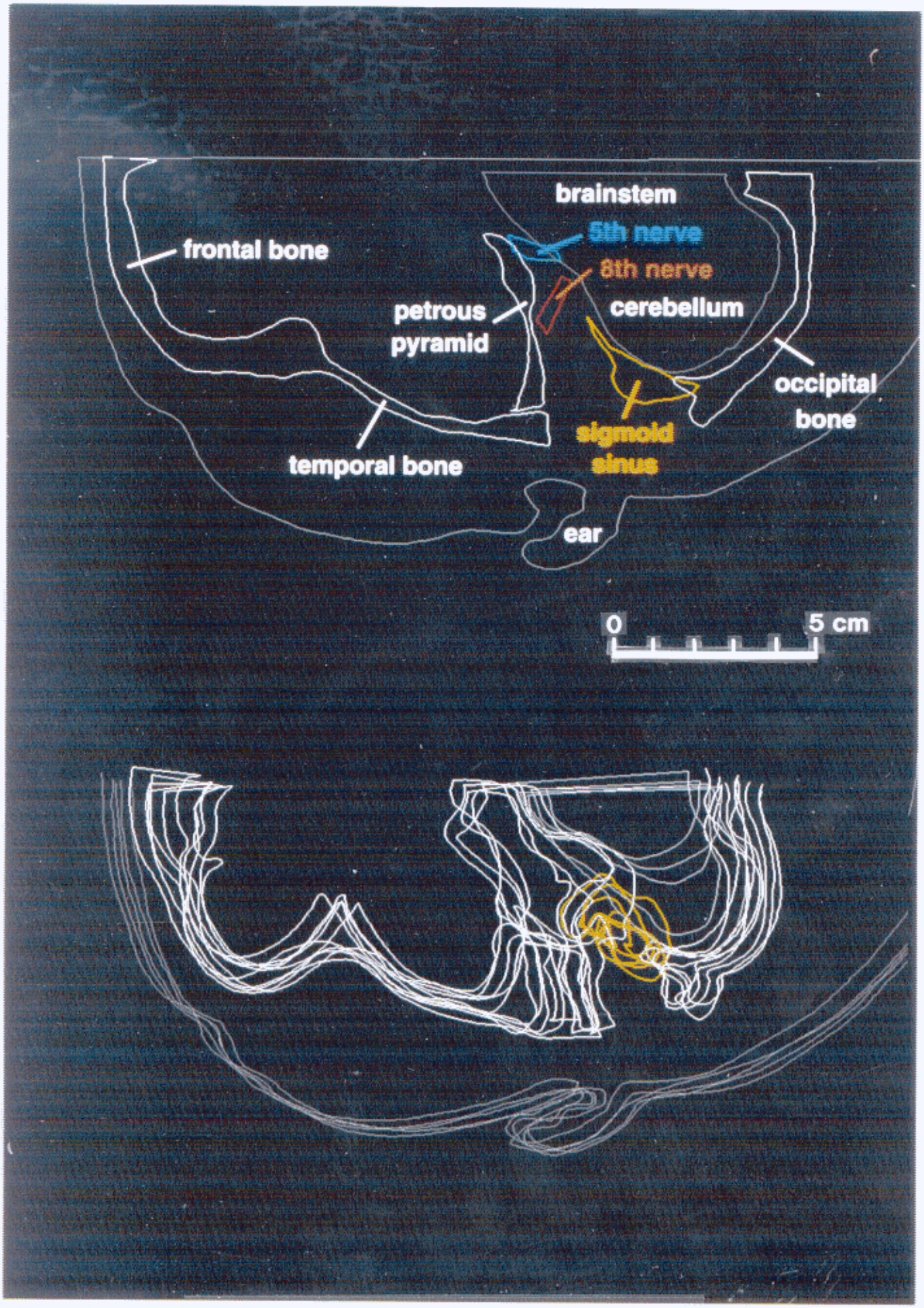

Fig 3.3a 3D reconstruction of CT images

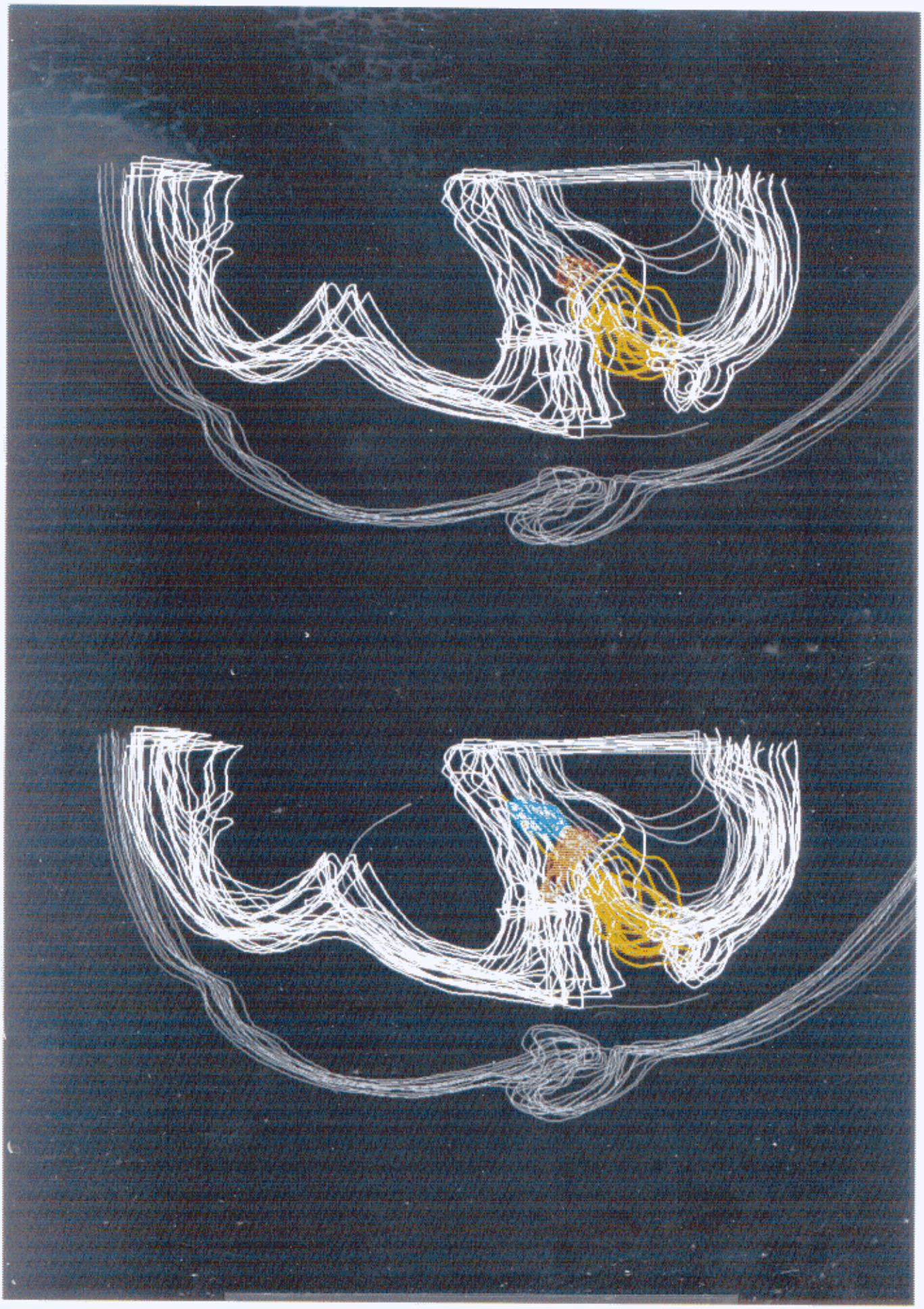

Fig 3.3b 3D reconstruction of CT images

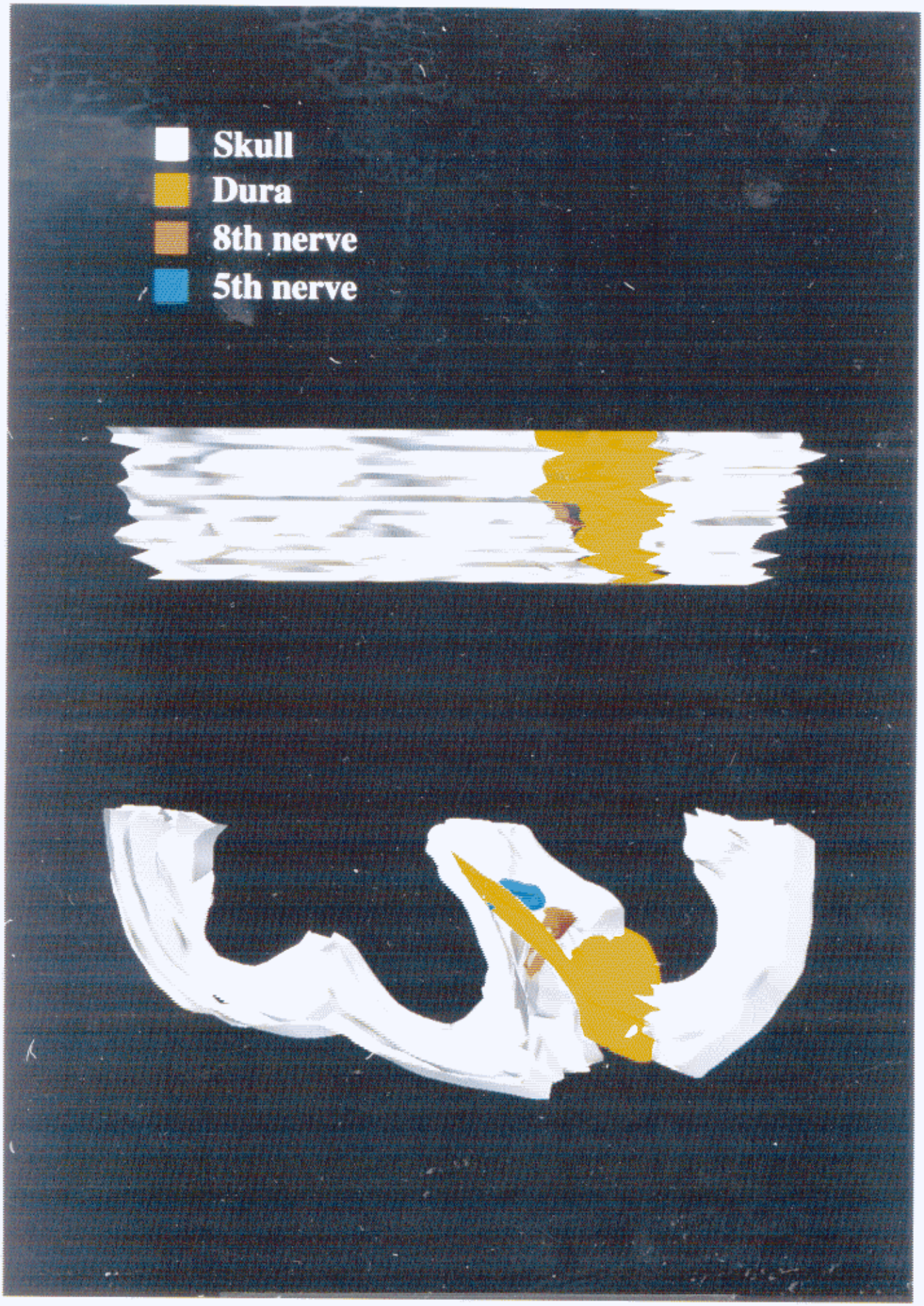

Fig 3.3c 3D reconstruction of CT images

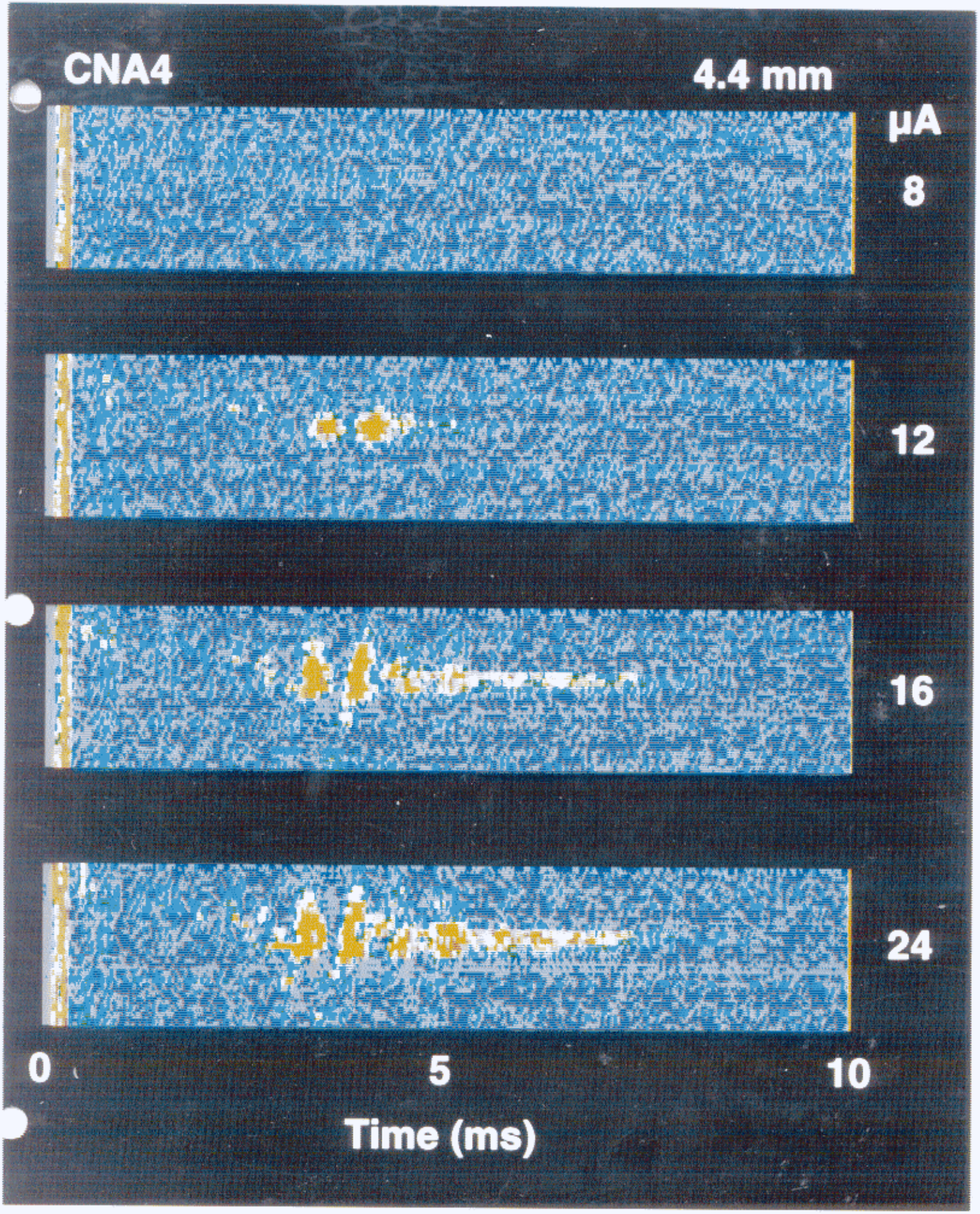
CNA4
4.4 mm
μA
8
12
16
24
0
5
10
Time (ms)

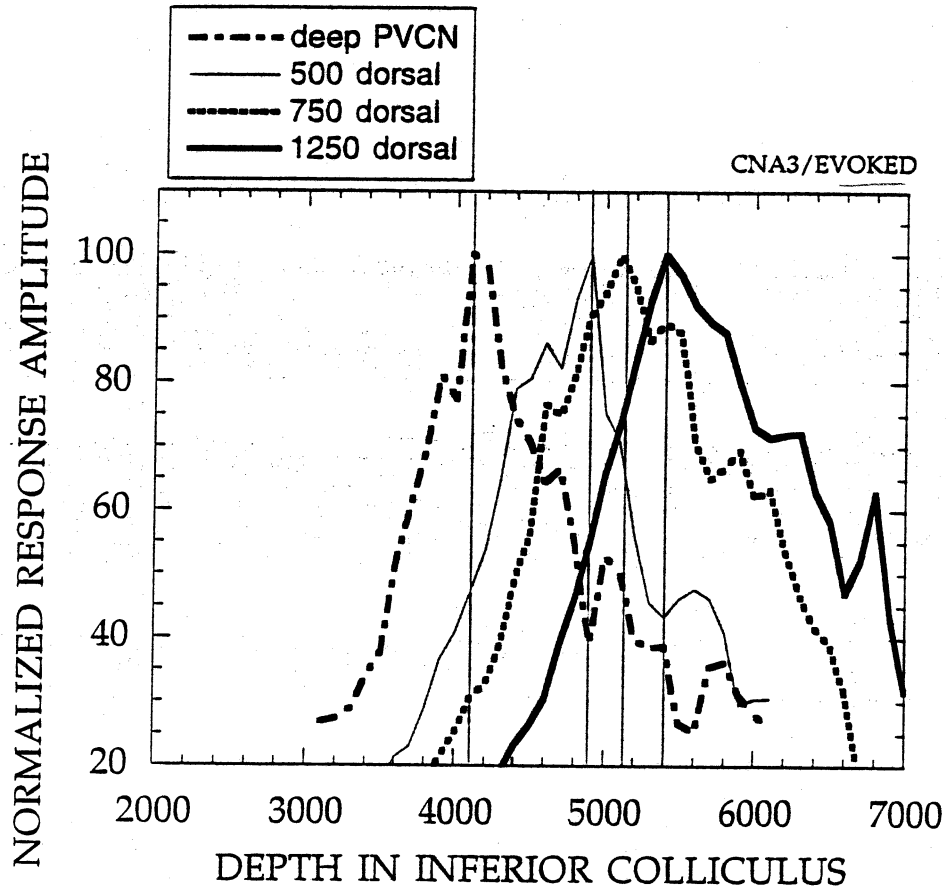
deep PVCN
500 dorsal
750 dorsal
1250 dorsal
CNA3/EVOKED
NORMALIZED RESPONSE AMPLITUDE
100
80
60
40
20
2000
3000
4000
5000
6000
7000
DEPTH IN INFERIOR COLLICULUS

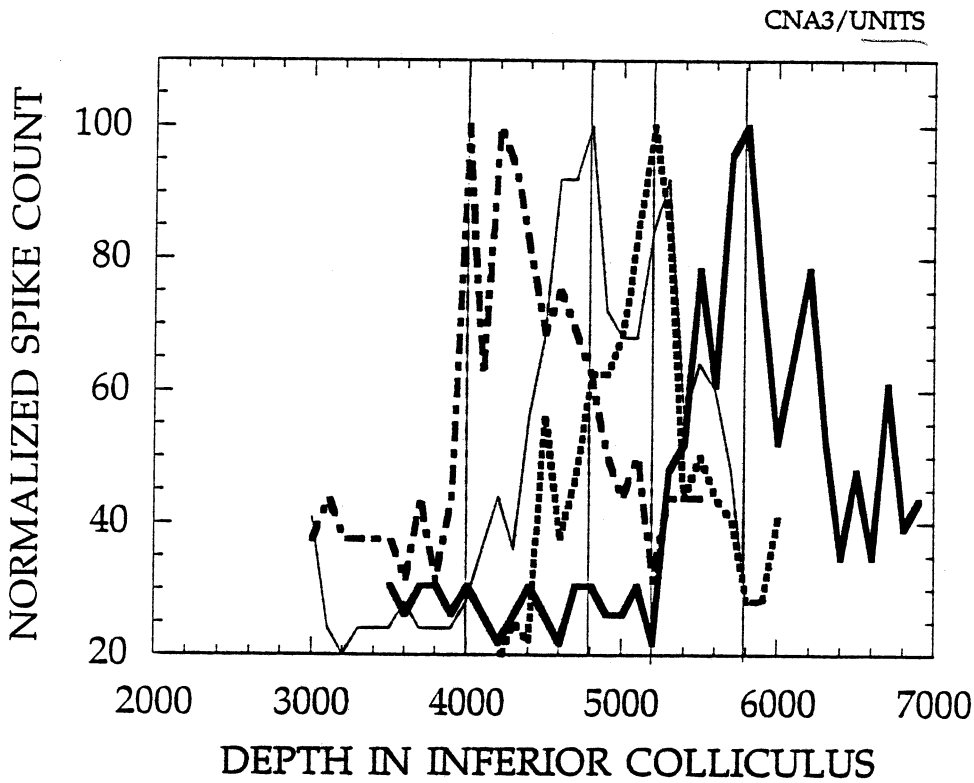
CNA3/UNITS
NORMALIZED SPIKE COUNT
100
80
60
40
20
2000
3000
4000
5000
6000
7000
DEPTH IN INFERIOR COLLICULUS

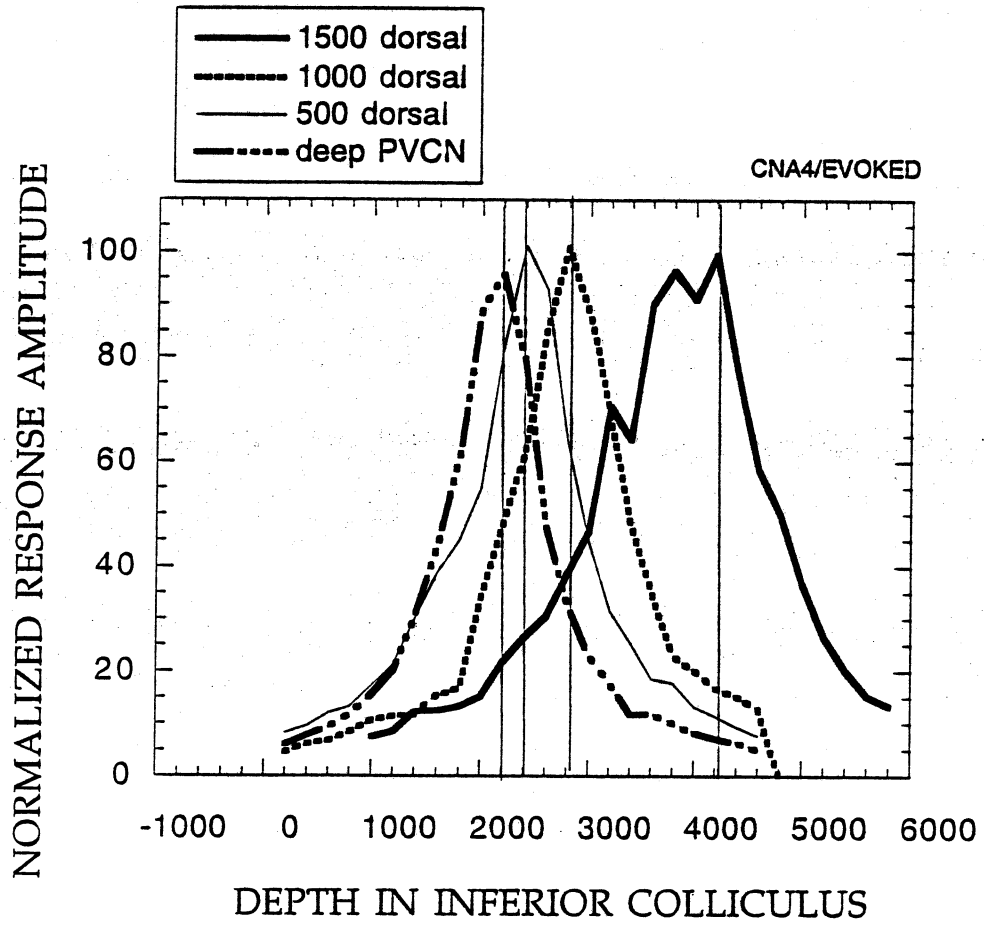
1500 dorsal
1000 dorsal
500 dorsal
deep PVCN
CNA4/EVOKED
NORMALIZED RESPONSE AMPLITUDE
0
20
40
60
80
100
-1000
0
1000
2000
3000
4000
5000
6000
DEPTH IN INFERIOR COLLICULUS

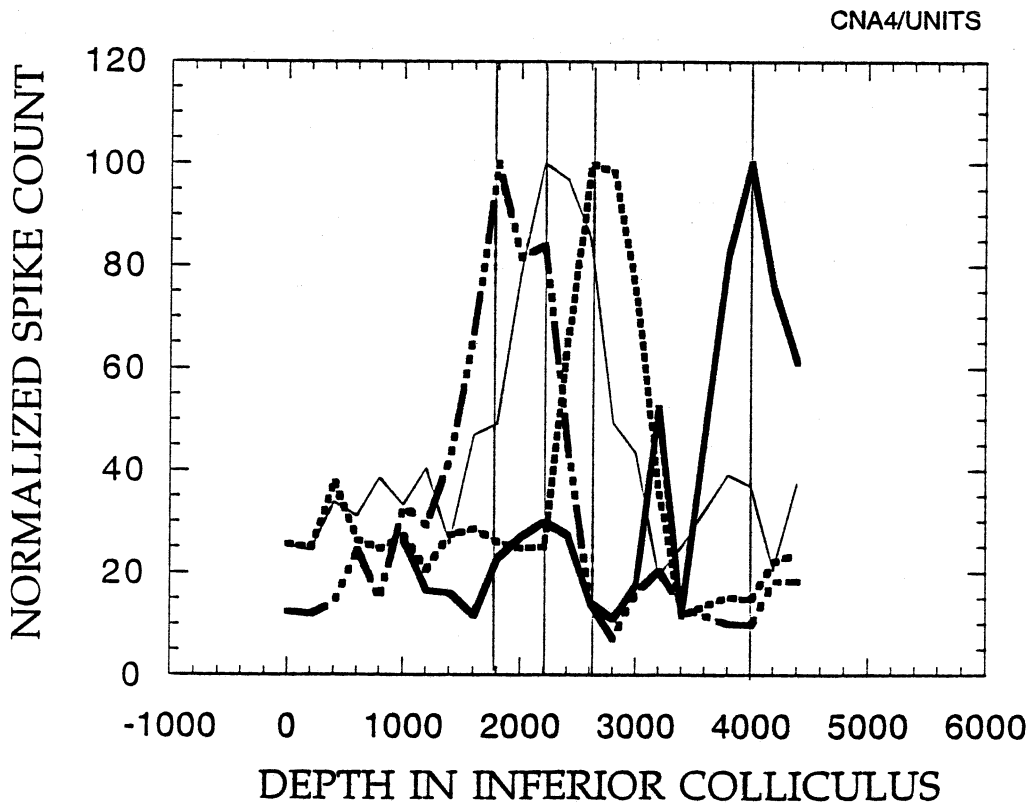
CNA4/UNITS
NORMALIZED SPIKE COUNT
0
20
40
60
80
100
120
-1000
0
1000
2000
3000
4000
5000
6000
DEPTH IN INFERIOR COLLICULUS

CNA3

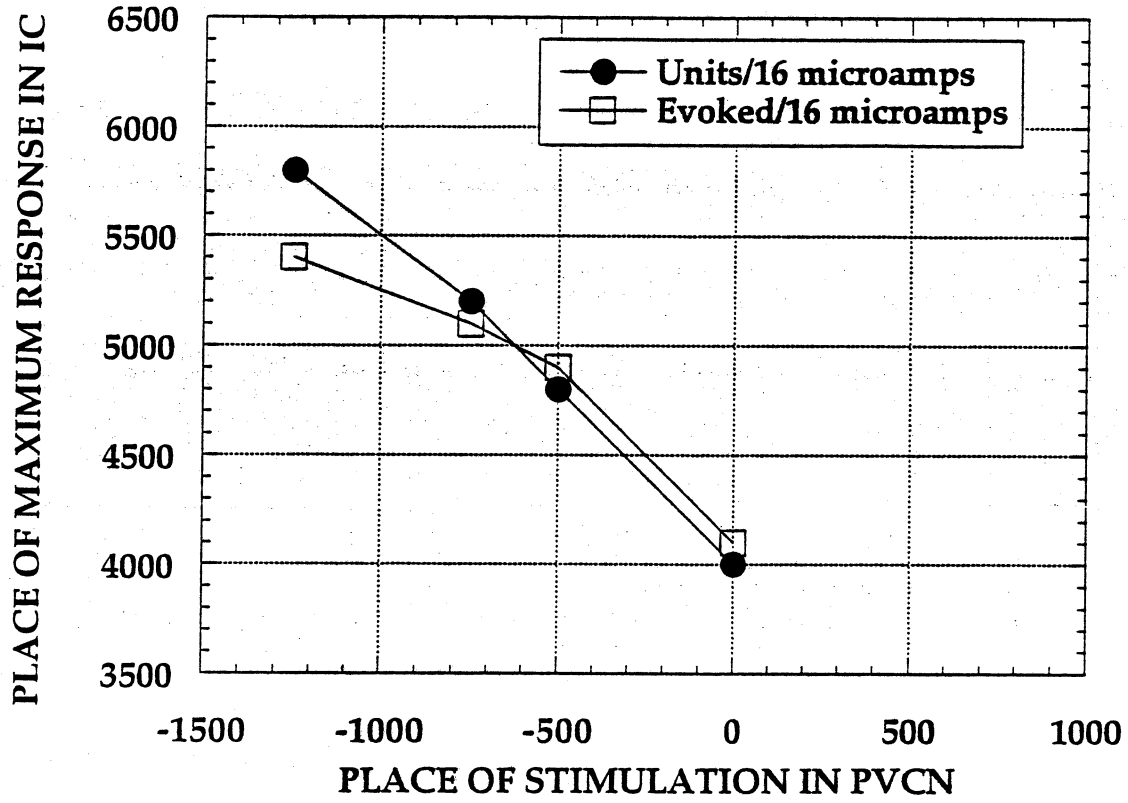
PLACE OF MAXIMUM RESPONSE IN IC
6500
6000
5500
5000
4500
4000
3500
Units/16 microamps
Evoked/16 microamps
-1500
-1000
-500
0
500
1000
PLACE OF STIMULATION IN PVCN

CNA4

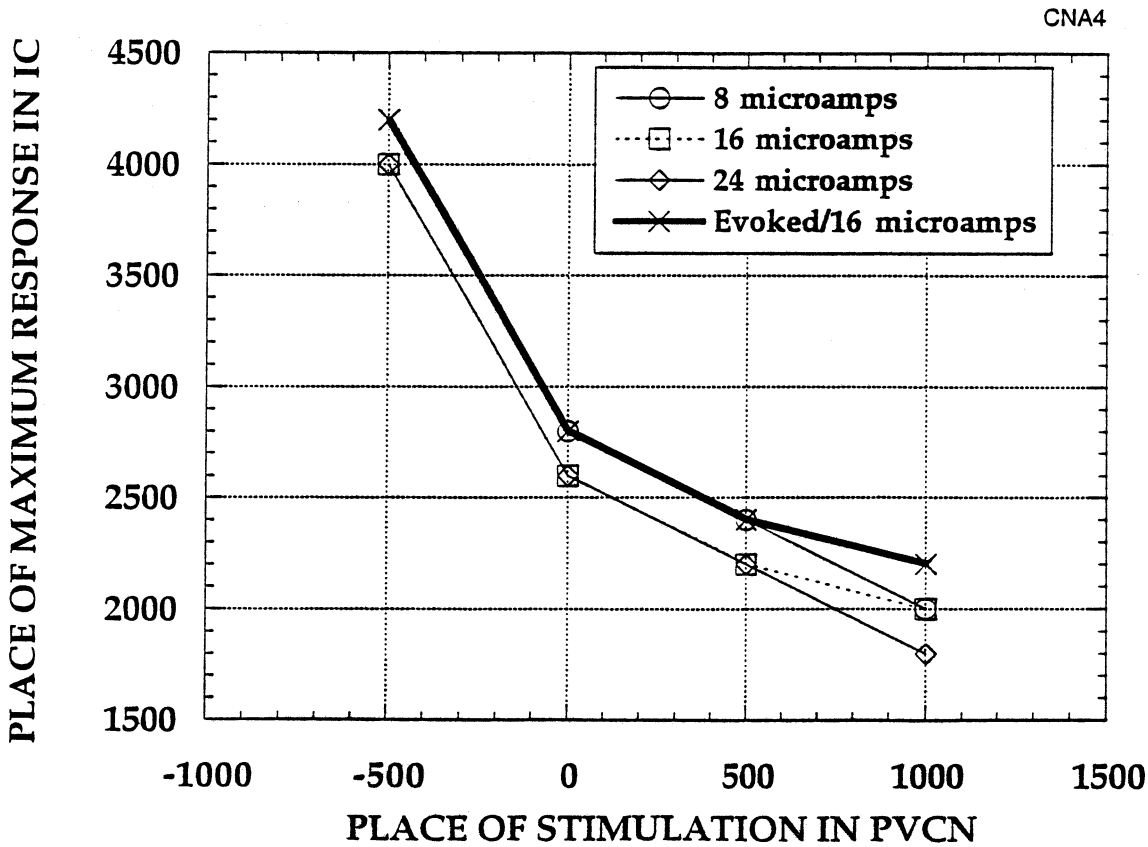
PLACE OF MAXIMUM RESPONSE IN IC
4500
4000
3500
3000
2500
2000
1500
8 microamps
16 microamps
24 microamps
Evoked/16 microamps
-1000
-500
0
500
1000
1500
PLACE OF STIMULATION IN PVCN

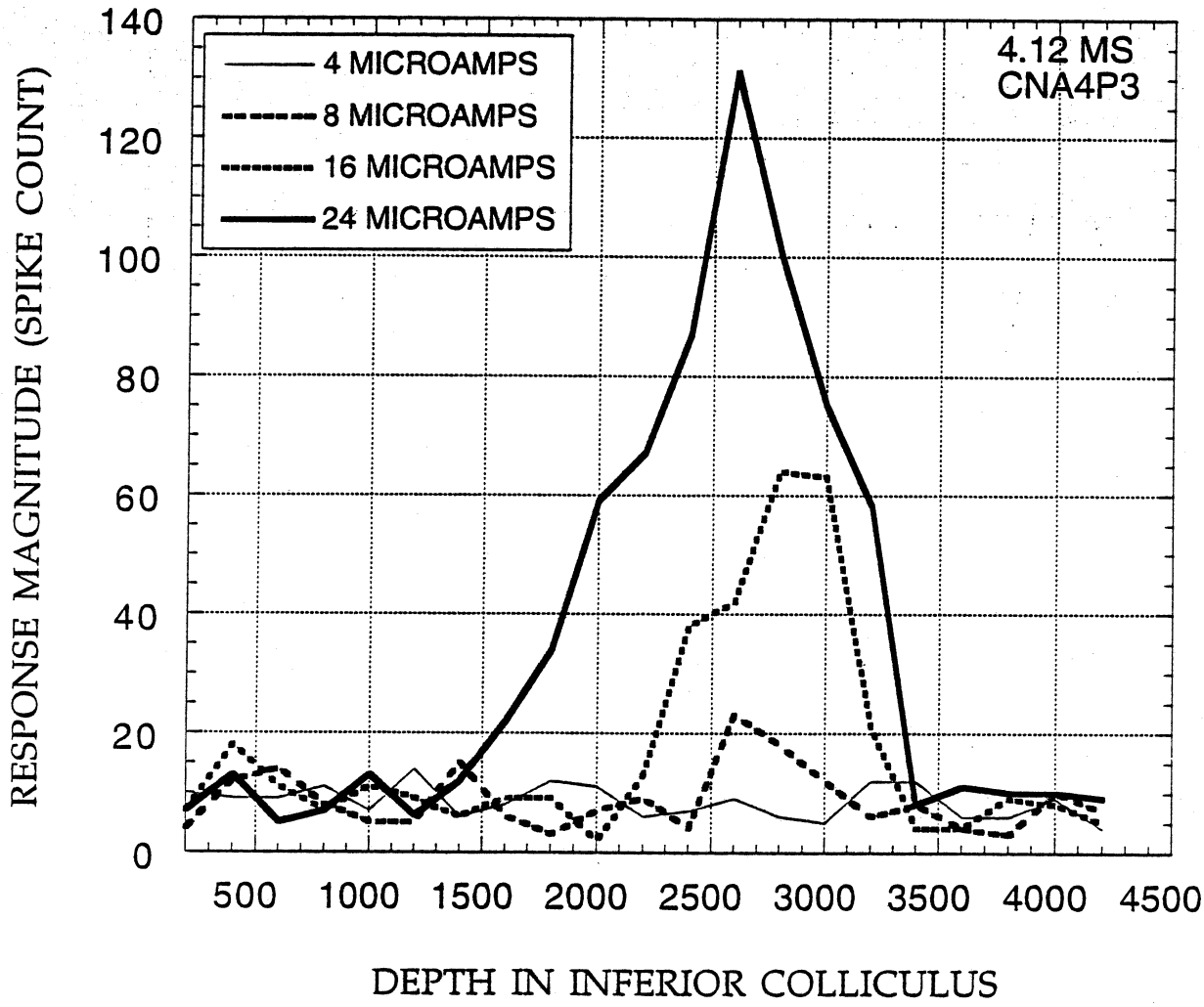
4 MICROAMPS
8 MICROAMPS
16 MICROAMPS
24 MICROAMPS
4.12 MS
CNA4P3
RESPONSE MAGNITUDE (SPIKE COUNT)
140
120
100
80
60
40
20
0
500
1000
1500
2000
2500
3000
3500
4000
4500
DEPTH IN INFERIOR COLLICULUS